15 April 1997

OPTICS COMMUNICATIONS

ELSEVIER

Optics Communications 137 (1997) 127–135

Full length article

Rigorous theory for axial resolution in confocal microscopes

P. Török [a,1], T. Wilson [b]

[a] *Multi-Imaging Centre, University of Cambridge, Downing Street, Cambridge CB2 3DY, UK*
[b] *Department of Engineering Science, University of Oxford, Parks Road, Oxford OX1 3PJ, UK*

Received 11 September 1996; accepted 25 November 1996

Abstract

We derive a rigorous theory for the imaging plane reflectors in confocal microscopes. The theory employs a full electromagnetic treatment that is applicable to lenses with high apertures. We show how the polarisation of the illuminating light and the size of either a coherent or an incoherent detector affects the axial resolution of the optical system. Numerical examples are also given for some important cases.

Keywords: Diffraction; High-aperture; Focusing; Vectorial theory; Scanning optical microscopy; Confocal microscopy

1. Introduction

One of the most useful techniques which serves both to check the alignment and to characterise the performance of a confocal scanning optical microscope is to measure the detected signal as a plane reflector is scanned through focus [1–3]. This axial or '$V(z)$' response exhibits a maximum when the reflector is positioned in the focal plane which then falls away rapidly as the defocus increases. This response both illustrates and quantifies the strength of the optical sectioning. It also confirms that only light which has originated from the focal region is detected efficiently. Since it is this property which allows the study of volume structures in three dimensions, it is very important to have a proper, rigorous, theoretical description of the axial response.

A theoretical description is available for finite sized incoherent detectors [3,4] but this is a scalar treatment which is only strictly applicable to low numerical aperture objective lenses. Recently Wilson and Tan [5] extended this analysis to high aperture lenses by using a vectorial treatment. However their approach was only valid for small axial deviations from the focal plane. It also used Fourier theory to describe the propagation of the electromagnetic field from the objective lens to the detector. In this paper we shall extend this analysis and develop a theory that is rigorous and whose solution satisfies Maxwell's equations. We shall also consider the use of both coherent and incoherent detectors of finite extent.

The construction of the paper is as follows. First we derive expressions for the strength vector and determine the apodisation function. Next the solution of the problem is given and our only assumption, ignoring vignetting, is discussed. We derive the axial detected signal response for a coherent and an incoherent detector and consider the special cases of an infinitely small or large detector. We then give numerical examples corresponding to the most important cases. Finally the most important features of our results are discussed.

2. Theory

The basis of our theory is as follows. We consider, for the sake of simplicity, a scanning microscope with a lens of finite tube length correction. In practice this requires that a 'point' source is placed at an axial position corresponding to the nominal tube length of the lens that produces a perfect spherical wave in the image space by

[1] Present address: Department of Engineering Science, University of Oxford, Parks Road, Oxford OX1 3PJ, UK. E-mail: peter.torok@eng.ox.ac.uk.

PII S0030-4018(96)00771-7

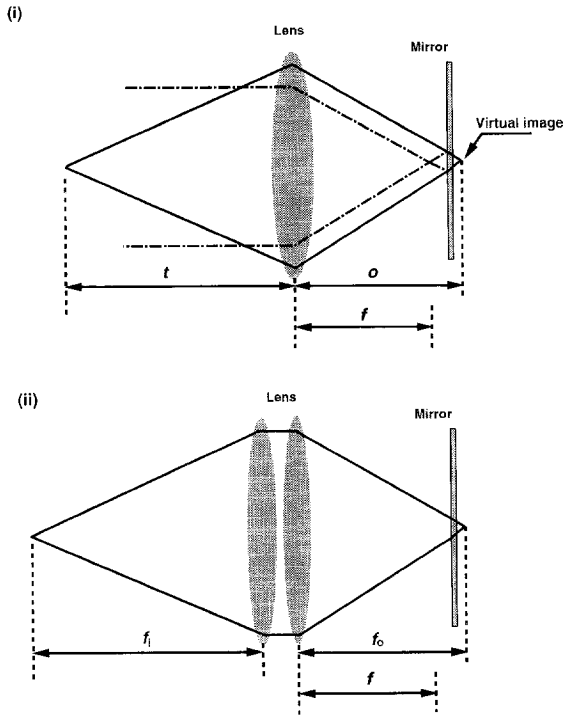

Fig. 1. Figure showing the illumination and the formation of the virtual probe (i) and the double lens decomposition of the detector lens (ii).

imaging the point source. In our theoretical model this lens is substituted by another lens that *focuses* a collimated incident illumination to the same axial (focal) position where the *imaging* lens would produce the intensity maximum. This we do to ease the calculations, but it is emphasised that this assumption does not restrict the validity of our theory. The focused field shall be referred to as the probe and hence the lens shall be referred to as the probe forming lens. The reflected light from the mirror produces a virtual image of the probe that is *imaged* by the detector lens into its image space, as shown in Fig. 1(i). For reflection scanning microscopes the probe forming and detector lenses are the same. The probe forming lens can be represented by a double-lens system [Fig. 1(ii)] where the lens closer to the mirror now possesses a *focal* length f_o equal to the object distance o of the single lens system and the lens farther from the mirror now possesses a *focal* length f_i equal to the image distance t of the single lens system. The lens closer to the mirror collimates the light and the lens farther from the mirror refocuses the light. It is, however, emphasised that this is only a theoretical construction designed to ease the use of our matrix formalism to be introduced below.

The linearly polarised coherent plane wave illumination incident upon the probe forming lens is converted into convergent and aberration free spherical waves. We will use the Debye-Wolf construction to represent the spherical waves as a sum of plane waves tangential to a particular spherical wavefront. We do this because the illumination is taken to be coherent and thus the principle of coherent superposition can be applied.

We decompose the electric vector field into tangential and radial components and use the matrix formalism, previously developed by Török et al. [6], to describe the electric vector field just before the mirror. The effect of the mirror on wave propagation is included by the use of the appropriate Fresnel amplitude reflection coefficients. Each plane wave is then propagated through the first lens [see Fig. 1(ii)] which can also be conveniently described by our matrix formalism. The second lens focuses the light and the electric vector is found, again, by using appropriate matrices. Finally the Cartesian co-ordinate components of the electric field in the focus region of the second lens, i.e. at the detector plane, are found.

2.1. The electric strength vector

For our decomposition, the usual assumptions are made, namely, that the electric vector maintains its direction with respect to a meridional plane and the electric vector remains on the same side of a meridional plane on passing through the system apart from reflection from the mirror. The illumination of the linearly polarised coherent and monochromatic plane wave incident upon the probe forming lens can be written as:

$$\boldsymbol{E}_0 = \begin{pmatrix} e_x \\ e_y \\ 0 \end{pmatrix} = \begin{pmatrix} \cos\gamma \\ \sin\gamma \\ 0 \end{pmatrix}, \tag{1}$$

where $e_x^2 + e_y^2 = 1$ and $\cos\gamma = e_x$ and $\sin\gamma = e_y$, with γ denoting the angle of the incident polarisation direction with respect to the positive x direction. In what follows we define matrix operators that are used to derive the electric field vector.

It will be convenient to define a co-ordinate system with spherical polar co-ordinates r, ϕ and θ that are defined so that $r > 0$, $0 \le \phi < \pi$ and $0 \le \theta < 2\pi$. For our treatment of the problem we decompose the electric vector into s- and p-polarised vector components, E_s and E_p respectively, and rotate the co-ordinate system such that the new co-ordinate system will contain components in the (p,s,ζ) system [6]. This co-ordinate system is defined in such a way that $E_\zeta = 0$. The electric vector components $\boldsymbol{E}_{br}$ after the lens are then in the following form:

$$\boldsymbol{E}_{br} = \mathbf{P}\mathbf{L}_1\mathbf{R}\boldsymbol{E}^{(0)}, \tag{2}$$

where the matrix $\mathbf{R}$ describes the co-ordinate transformation for rotation around the z axis:

$$\mathbf{R} = \begin{pmatrix} \cos\theta & \sin\theta & 0 \\ -\sin\theta & \cos\theta & 0 \\ 0 & 0 & 1 \end{pmatrix}, \tag{3}$$

and the matrix **L** describes the changes in the electric field as it traverses the lens (the subscript indicates whether the matrix describes the effect of the first lens – 1 – or that of the second lens – 2 – of the double-lens system):

$$\mathbf{L} = \begin{pmatrix} \cos\phi & 0 & \sin\phi \\ 0 & 1 & 0 \\ -\sin\phi & 0 & \cos\phi \end{pmatrix}. \tag{4}$$

The matrix **P** describes the co-ordinate system rotation which generates E_s and E_p components with $E_\zeta = 0$:

$$\mathbf{P} = \begin{pmatrix} \cos\phi & 0 & -\sin\phi \\ 0 & 1 & 0 \\ \sin\phi & 0 & \cos\phi \end{pmatrix}. \tag{5}$$

The refraction on the mirror can be described, in the (p,s,ζ) system, by

$$\mathbf{I} = \begin{pmatrix} r_p & 0 & 0 \\ 0 & -r_s & 0 \\ 0 & 0 & r_p \end{pmatrix}, \tag{6}$$

where r_p and r_s are the Fresnel reflection coefficients [7]:

$$r_p = \frac{\cos\phi' - n\sqrt{1-n^2\sin^2\phi'}}{\cos\phi' + n\sqrt{1-n^2\sin^2\phi'}},$$

$$r_s = \frac{n\cos\phi' - \sqrt{1-n^2\sin^2\phi'}}{n\cos\phi' + \sqrt{1-n^2\sin^2\phi'}},$$

where $n = n_1/n_2$ with n_1 and n_2 represent the refractive indices of the medium of propagation and the plane reflector, respectively and ϕ' is the azimuthal angle in the image space. The electric field vector, after refraction, traverses the lens again and in the space between the two lenses is in the form:

$$\boldsymbol{E}_{al} = \mathbf{L}_1^{-1}\mathbf{P}^{-1}\mathbf{I}\boldsymbol{E}_{br}. \tag{7}$$

We note that in the above equation the electric field is still expressed in the (p,s,z) system. Finally the electric field vector after being focused by the second lens is given in the (x,y,z) system by

$$\boldsymbol{E}_2 = \mathbf{R}^{-1}\mathbf{L}_2\boldsymbol{E}_{al}, \tag{8}$$

or,

$$\boldsymbol{E}_2 = c(\phi)\,\mathbf{R}^{-1}\mathbf{L}_2\mathbf{I}\mathbf{R}\boldsymbol{E}^{(0)}, \tag{9}$$

where we have introduced a factor $c(\phi)$ to account for the apodisation and used

$$\mathbf{P}\mathbf{L}_1 = \mathbf{L}_1^{-1}\mathbf{P}^{-1} = \begin{pmatrix} 1 & 0 & 0 \\ 0 & 1 & 0 \\ 0 & 0 & 1 \end{pmatrix}.$$

We shall return to the precise form of the apodisation factor, $c(\phi)$, later.

2.2. The electric field

It was shown by Wolf [8] that for a high Fresnel number lens the electric field can be obtained as a superposition of plane waves. Luneburg [9] proved that Wolf's representation is an exact solution of the Maxwell's equation and thus our treatment also satisfies Maxwell's equations. This approach is mathematically equivalent to the angular spectrum representation of plane waves. We shall make an approximation in obtaining the solution, namely that vignetting is ignored, but, as shown below, this approximation introduces negligible error into the formulation.

The fundamental solution for the electric field is given by:

$$\boldsymbol{E} = -\frac{i\kappa}{2\pi}\int\int_{\Omega}\frac{\boldsymbol{A}(s_x,s_y)}{s_z}\exp(i\kappa\psi) \times\exp\left[i\kappa(s_x x + s_y y + s_z z)\right] ds_x\, ds_y, \tag{10}$$

where $\kappa = n_1 2\pi/\lambda = nk_0$ is the wavenumber, $s = (s_x,s_y,s_z)$ is the wave vector, Ω is the convergence angle of the lens, $\boldsymbol{A}(s_x,s_y)$ is a strength vector and $\exp(i\kappa\psi)$, with $\psi = f(\phi)$, is an arbitrary phase term, to be determined below.

After transforming Eq. (10) into spherical and cylindrical polar co-ordinate system and representing the wave vector by

$$\boldsymbol{s} = \sin\phi\cos\theta\,\boldsymbol{i} + \sin\phi\sin\theta\,\boldsymbol{j} + \cos\phi\,\boldsymbol{k}, \tag{11}$$

and the position vector by

$$\boldsymbol{r}_p = \rho\cos\theta_p\,\boldsymbol{i} + \rho\sin\theta_p\,\boldsymbol{j} + z\boldsymbol{k}, \tag{12}$$

where $\boldsymbol{i}$, $\boldsymbol{j}$ and $\boldsymbol{k}$ are the unit base vectors of the (x,y,z) orthogonal system, we obtain:

$$\boldsymbol{E} = -\frac{i\kappa}{2\pi}\int_0^{\alpha}\int_0^{2\pi}\boldsymbol{A}(\phi,\theta)\sin\phi \times\exp\left[i\kappa\rho\sin\phi\cos(\theta-\theta_p)\right] \times\exp(i\kappa\psi)\exp(i\kappa z\cos\phi)\,d\phi\,d\theta, \tag{13}$$

where α is the convergence semi-angle of the second lens. The strength vector in Eq. (13) is given by Eq. (9), yielding:

$$\boldsymbol{A}(\phi,\theta) = c(\phi) \times\begin{pmatrix} r_p\cos(\theta-\gamma)\cos\phi\cos\theta - r_s\sin(\theta-\gamma)\sin\theta \\ r_p\cos(\theta-\gamma)\cos\phi\sin\theta + r_s\sin(\theta-\gamma)\cos\theta \\ -r_p\sin\phi\cos(\theta-\gamma) \end{pmatrix}. \tag{14}$$

After some straightforward manipulation and by using [10]

$$\int_0^{2\pi} \begin{matrix}\cos n\phi \\ \sin n\phi\end{matrix} \exp[\mathrm{i}\rho\cos(\phi-\zeta)]\,\mathrm{d}\phi = 2\pi \mathrm{i}^n J_n(\rho) \begin{matrix}\cos n\zeta \\ \sin n\zeta\end{matrix}$$

where $J_n(\ )$ is the Bessel function, zero kind, order n, we obtain the Cartesian components of the electric field:

$$E_x = -\frac{\kappa}{2}\left[\cos\gamma\,(I_0 + I_2\cos 2\theta_p) + \sin\gamma\, I_2 \sin 2\theta_p\right],$$

$$E_y = -\frac{\kappa}{2}\left[\cos\gamma\, I_2 \sin 2\theta_p + \sin\gamma\,(I_0 - I_2\cos 2\theta_p)\right],$$

$$E_z = -\mathrm{i}\kappa\left[\cos\gamma\, I_1\cos\theta_p + \sin\gamma\, I_1 \sin\theta_p\right], \tag{15}$$

where

$$I_0 = \int_0^{\alpha} c(\phi)\,(r_s - r_p\cos\phi)\sin\phi\, J_0(\kappa\rho\sin\phi) \times\exp(\mathrm{i}\kappa\psi)\exp(\mathrm{i}\kappa z\cos\phi)\,\mathrm{d}\phi,$$

$$I_1 = \int_0^{\alpha} c(\phi)\, r_p \sin^2\phi\, J_1(\kappa\rho\sin\phi)\exp(\mathrm{i}\kappa\psi) \times\exp(\mathrm{i}\kappa z\cos\phi)\,\mathrm{d}\phi,$$

$$I_2 = \int_0^{\alpha} c(\phi)\,(r_s + r_p\cos\phi)\sin\phi\, J_2(\kappa\rho\sin\phi) \times\exp(\mathrm{i}\kappa\psi)\exp(\mathrm{i}\kappa z\cos\phi)\,\mathrm{d}\phi. \tag{16}$$

2.3. The apodisation function

In order to be able to incorporate the apodisation to our formalism an apodisation function has been introduced in Eq. (9). Microscope objective lenses are usually designed to satisfy Abbe's sine condition and have a functional form $c = \sqrt{\cos\phi'}$ [11]. When the lens satisfies the Herschel condition $c = 1$ [11]. In this paper we assume that the lens satisfies the sine condition. It is clear that, since the same lens is used for forming the probe and to collect the reflected light, this function needs to be considered twice, once for the probe formation and one for the detection, thus giving an overall apodisation function of $c = \cos\phi'$. Since we assumed that the lens satisfies the sine condition is easy to find the relationship between ϕ, the azimuthal angle in the image space of the detector lens, and ϕ', the azimuthal angle in the image space of the probe forming lens [11]:

$$\frac{n\sin\phi}{n'\sin\phi'} = \beta,$$

where β is the differential (or transverse) magnification which, as we will show below, is a function of the mirror defocus, d. The above expression yields for homogeneous object and image spaces

$$\sin\phi' = \beta(d)\sin\phi, \quad \cos\phi' = \sqrt{1-\beta^2(d)\sin^2\phi}\,. \tag{17}$$

2.4. The image location

In the following our considerations shall be confined to the accuracy of Gaussian optics. The origin of the co-ordinate system, due to the definition of the problem, coincides with the intersection of the optical axis and the image plane. This means that the origin of the co-ordinate system is shifted with the mirror defocus. When the image of the object is at an axial location equal to the nominal tube length we can write the lens law as:

$$\frac{1}{t} + \frac{1}{o} = \frac{1}{f}, \tag{18}$$

where t is the tube length, o is the object distance and f is the focal length of the detector lens. When the mirror is defocused the lens images a virtual probe. The change in axial location of the virtual image is $2d$ for a mirror defocus of d. The image position of the defocused probe is denoted by t' and thus the lens law gives:

$$\frac{1}{t'} + \frac{1}{o+2d} = \frac{1}{f}. \tag{19}$$

For a given lens the tube and focal lengths, t and f, respectively, are known. The object distance can thus be calculated from Eq. (18) and substituted into Eq. (19), from which the modified image position, corresponding to a mirror defocus of d, is given by:

$$t' = \frac{f[2d(t-f)+ft]}{f(f-2d)+2dt}. \tag{20}$$

When a detector is employed in this system its axial position does not, of course, vary with the defocus of the mirror. The detector is always placed at an axial position corresponding to the nominal tube length t of the lens.

For imaging systems the magnification, β, is defined as the ratio of the *actual* image and object distances, t' and o', respectively:

$$\beta = \frac{t'}{o'} = \frac{t'}{o+2d}, \tag{21}$$

from which, together with Eq. (20) we obtain:

$$\beta = \frac{\beta_{\mathrm{nom}}}{1+(2d/t)\beta_{\mathrm{nom}}(\beta_{\mathrm{nom}}+1)}, \tag{22}$$

where β_{nom} denotes the nominal magnification for a mirror defocus of $d = 0$. We note that the magnification is a function of mirror defocus and that for high magnification objectives $\beta(d) \neq \beta(-d)$. If we consider a typical micro-

scope objective lens (Leica, $t = 160$ mm, $\beta_{nom} = 63$, NA $= 0.9$) then we find for $d = -10$ μm, $\beta = 1.33\beta_{nom} = 84$ and for $d = +10$ μm, $\beta = 0.8\beta_{nom} = 50.4$. However for distances within the optical sectioning range we find for $d = 0.3$ μm, $\beta = 0.985\beta_{nom} = 62$ whereas for $d = -0.3$ μm, $\beta = 1.015\beta_{nom} = 64$ and hence this effect is likely to have an important effect on the structure of the axial side lobes.

It now remains to find an expression for the defocus, z, at the detector. This is given by the axial distance between t and t'

$$z = -2d\beta_{nom}\beta(d), \tag{23}$$

and we see that the axial magnification reduces to β_{nom}^2 for small mirror displacements, d.

The integration angle α is also a function of the mirror defocus. It follows from the sine condition (17), to a good approximation, that

$$\sin\alpha \simeq \alpha \simeq \frac{NA}{\beta(d)}. \tag{24}$$

For the above numerical example α (in radians) is given for $d = -5$ μm by $\alpha = 0.0107$ and for $d = +5$ μm by $\alpha = 0.018$.

For lenses with finite tube length correction the lens produces an aberration free image when the actual object distance satisfies the lens law (18). When the object is placed at a distance different from o the image appears at t' and the phase front propagating towards the detector will suffer from third-order spherical aberration [12] provided that the paraxial approximation applies to the *image* space of the lens and the sine condition is satisfied. We note that when the lens satisfies the Herschel condition the aberration vanishes. The assumption of paraxial approximation in the image space is clearly justified in practice for high NA lenses with finite (usually 160–210 mm) tube length.

The phase error of the aberration is given by Sheppard and Gu [12] as

$$\psi = 4d\sin^4(\phi/2), \tag{25}$$

which represents the additional phase term [2] in Eq. (16). Clearly, when $d = 0 \Rightarrow t' = t$ and thus the mirror is 'in focus' the phase error vanishes.

Eq. (15) together with Eqs. (16), (22)–(25) constitute the rigorous solution of our problem.

2.5. The effect of vignetting

Here we will consider the effect of vignetting from two different points of view. First we show that vignetting causes a negligible intensity decrease for *negative* defoci together with a negligible numerical aperture decrease for *positive* defoci. For the sake of simplicity in the following a focusing lens is considered as shown in Fig. 2.

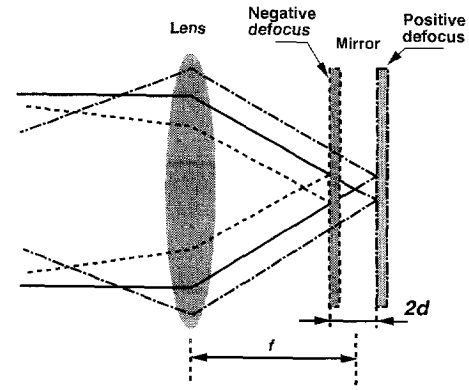

Fig. 2. Figure illustrating the effect of vignetting. This case is considered, for simplicity, for a focusing lens.

Positive defocus (i.e. the focus is situated between the lens and the mirror) clearly does not affect the *total* intensity collected by the lens. When negative defocus occurs a simple geometrical optics approach gives a reasonable estimate for the intensity decrease. The power density at the right hand side of the lens for the illumination is given by $P_i = ca^2\pi$, where c is some constant and a is the radius of the lens. The power density of the reflected light at the right hand side of the lens is given by $P_r = c\pi(f-2d)^2\tan^2\alpha$. The ratio of the two power densities determines, in our simple model, the light loss due to defocusing. Assuming now a lens numerical aperture of 0.9 it is easy to show that for $d = -10$ μm defocus the relative power density decreases only by 0.8% that, as shown below, is negligible with respect to those changes introduced by diffraction.

The negative defocus clearly does not affect the effective numerical aperture of the system. For positive defoci the effective numerical aperture is decreased due to a limitation of the effective lens aperture. The effective numerical aperture of the system, based on geometrical optics, is given by

$$NA_{eff} = \frac{(f-2d)\tan\alpha}{\left[f^2 + (f-2d)^2\tan^2\alpha\right]^{1/2}},$$

which results in an effective numerical aperture decrease, again for NA = 0.9, of 0.64% for $d = 10$ μm. This can also be considered to be negligible.

3. Axial signal of the defocused mirror

In this section we derive expressions for the axial intensity signal of a scanning microscope employing either

[2] Note that, due to the definition of the co-ordinate system, the sign of this phase factor is opposite to that given by Sheppard and Gu [12].

an incoherent or a coherent detector. The size of the detector is also considered.

3.1. Incoherent detectors

When incoherent detection is employed the *intensity* of the light is detected and the image signal is proportional to the integral of the light intensity over the area of the detector. Although in the following calculation we shall assume that the detector is centered on the optical axis, it is straightforward to take into consideration a detector offset or misalignment. The detected signal I_i is given by

$$I_i(z) = \int_{D_i} |\boldsymbol{E}|^2 S_i \, \mathrm{d}D_i,$$

where D_i is the area and S_i is the sensitivity of the incoherent detector and, from Eqs. (15) and (16)

$$\begin{aligned} |\boldsymbol{E}|^2 &= E_x E_x^* + E_y E_y^* + E_z E_z^* \\ &= |I_0|^2 + 2\Re\left(I_0 I_2^*\right)\cos\left[2(\gamma - \theta_p)\right] + |I_2|^2 \\ &\quad + 2|I_1|^2 \cos^2(\gamma - \theta_p), \end{aligned} \tag{26}$$

and thus

$$I_i(z) = \int_0^R \left(|I_0|^2 + 2|I_1|^2 + |I_2|^2\right) \rho \, \mathrm{d}\rho, \tag{27}$$

where $*$ denotes the complex conjugation, R is the radius of the detector aperture and we have ignored the constant multipliers. We note that the kernel of the above equation is formally identical to that obtained by Richards and Wolf [13] for the *total* energy density of the field in the focal region of a high aperture lens (differences, of course, being present for the I_n integrals). Eq. (27) shows that the incoherent axial intensity distribution is independent of the incident polarisation direction. It should be emphasised that this only applies when the detector is centered on the axis. When the detector size is extended to the infinity $R \to \infty$ the above expression readily gives the axial distribution that is independent of the axial position of the mirror, as anticipated.

3.2. Coherent detectors

When coherent detection is considered the *amplitude* of the field is detected, thus the coherent detected signal $I_c(z)$ is given by

$$I_c(z) = \left| \int_{D_c} \boldsymbol{E} S_c \, \mathrm{d}D_c \right|^2,$$

where S_c is the sensitivity of the coherent detector. The integration over the coherent detector D_c yields zero for terms in Eq. (15) consisting of $\sin\theta_p$, $\sin 2\theta_p$, $\cos\theta_p$ and $\cos 2\theta_p$ and thus

$$\begin{aligned} I_c(z) &= \left| \cos\gamma \int_0^R I_0 \, \rho \, \mathrm{d}\rho + \sin\gamma \int_0^R I_0 \, \rho \, \mathrm{d}\rho \right|^2 \\ &= \left| (\cos\gamma + \sin\gamma) \int_0^R I_0 \, \rho \, \mathrm{d}\rho \right|^2, \end{aligned} \tag{28}$$

which gives:

$$\begin{aligned} I_c(z) = \frac{R^2}{\kappa^2}(1 + \sin 2\gamma) \Bigg| & \int_0^\alpha c(\phi)\left(r_s - r_p \cos\phi\right) \\ & \times \exp(\mathrm{i}\kappa\psi)\exp(\mathrm{i}\kappa z \cos\phi) \\ & \times J_1(\kappa R \sin\phi)\, \mathrm{d}\phi \Bigg|^2, \end{aligned} \tag{29}$$

where, again, we have ignored the constant multipliers. When the detector becomes infinitely small the detected signal can directly be derived from Eq. (16). For $\rho = 0$, $I_1 = I_2 = 0$ and thus

$$\begin{aligned} I_c(z) = (1 + \sin 2\gamma) \Bigg| & \int_0^\alpha c(\phi)\left(r_s - r_p \cos\phi\right) \\ & \times \sin\phi \exp(\mathrm{i}\kappa\psi)\exp(\mathrm{i}\kappa z \cos\phi)\, \mathrm{d}\phi \Bigg|^2. \end{aligned} \tag{30}$$

The above equation shows that the strength of the coherent axial signal does depend on the direction of incident polarisation. When the incident polarisation coincides with the 0 or 90° direction the peak signal is half as strong as the peak signal corresponding to the $\gamma = 45°$ direction.

3.3. The electric field of coherent detection

In the previous subsection we have considered a detector that is sensitive to electric field $\boldsymbol{E}$ rather than intensity. Eq. (28) describes the detected signal from a uniform coherent electric field detector. We now calculate this signal when $R \to \infty$, i.e. the *total* electric field is determined on an arbitrary (x, y) plane. The order of integration in Eq. (28) is interchangeable because the integrand is continuous on $(0 \le \phi \le \alpha)$ and $(0 \le \rho \le R)$. By gathering the ρ dependent terms we obtain

$$\lim_{R \to \infty} \int_0^R J_0(\kappa\rho \sin\phi)\, \rho \, \mathrm{d}\rho = 0,$$

which means that when the integration is extended to the infinity, and thus the total electric field is considered on an arbitrary (x, y) plane, *the detector signal vanishes*. It is easy to show that this statement would also apply to a detector sensitive to the magnetic field. The above equation is valid as long as the sensitivity distribution of the detector is unity throughout its diameter. When, for example, the detector possesses a Gaussian sensitivity, as would be the case when a single mode optical fibre was used as a

coherent detector then the above expression is modified and yields (with b arbitrary real constant):

$$\lim_{R\to\infty}\int_0^R \exp\left(-\frac{\rho^2}{b^2}\right) J_0(\kappa\rho\sin\phi)\,\rho\,\mathrm{d}\rho = \frac{b\sqrt{\pi}}{2} \times I_0\left(\frac{-b^2\kappa^2\sin^2\phi}{8}\right)\exp\left(\frac{-b^2\kappa^2\sin^2\phi}{8}\right)\neq 0,$$

where $I_0(\ )$ is the modified Bessel function, zero kind, order zero. In this case the signal does not vanish.

4. Numerical results

The numerical results were computed for a Leitz (Wetzlar) objective lens (NPL Fluotar, $t = 160$ mm, $\beta_{\mathrm{nom}} = 63\times$, NA = 0.9), for light of wavelength $\lambda = 488$ nm and for a gold plated plane mirror ($n_2 = 0.24 - i2.78$). The lens and the mirror were assumed to be embedded in air. For numerical computations programs were written using the FORTRAN 77 programming language with NAG (Numerical Algorithm Group, Oxford) subroutines and the programs were run on an IBM compatible 486DX2 66MHz computer. Numerical results were then plotted by the Tecplot software. No post processing of computed data was performed, apart from normalisation.

4.1. Incoherent detection

Fig. 3(a) shows the results of numerical computations obtained by using Eqs. (27) and (16). The intensity is given in arbitrary units but individual curves can directly be compared. All the curves exhibit slight asymmetry with respect to the zero mirror defocus position. This asymmetry is caused by the following factors:

1. dependence of the spherical aberration, represented by Eq. (25), on mirror defocus
2. dependence of the system magnification β, represented by Eq. (22), on mirror defocus
3. dependence of the integration angle α, represented by Eq. (24), on mirror defocus
4. nonlinear dependence of the axial position z, represented by Eq. (23), on mirror defocus

It is important to note that 4 itself would be sufficient to produce an asymmetrical axial response, but each of the above terms contribute to the final distribution. We also note that the spherical aberration would not produce asymmetrical axial response as shown by Sheppard and Gu [12]. The asymmetrical axial response of a scanning optical microscope has long been shown experimentally [1] but, to the best of the authors' knowledge, no prior high aperture theory publications have ever reported on its theoretical confirmation. It is stated here, but only proved in a following publication, that any deviations from the nominal tube length of the lens results in even more pronounced asymmetrical behaviour.

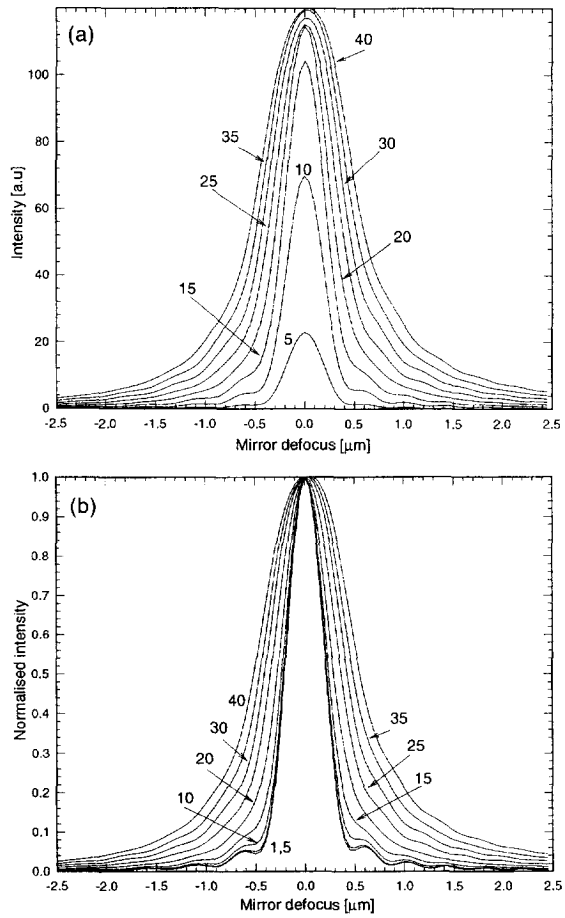

Fig. 3. Axial scans of the detected intensity for an incoherent detector (a). (b) Corresponds to the same case but individual curves are normalised to the unity. The radius of the detector is given in μm.

The individual curves in Fig. 3(a) exhibit a monotonic increase in peak intensity, this increase being more pronounced for smaller detector diameters and being less pronounced for large detector sizes. This finding is in complete agreement with previous works by Wilson and Carlini [3,4] which were based on the scalar paraxial theory.

When the individual curves are normalised to the unity [Fig. 3(b)] the increase of the distribution width with increasing detector radius becomes apparent. The width does not change significantly for detector radii of 1, 5 and 10 μm but for larger detector radii the effect is significant. This fact is also in agreement with previous work [3,4] based on the scalar paraxial theory.

4.2. Coherent detection

In Fig. 4 we show normalised axial distributions of the detected signal for a coherent detector. This figure exhibits

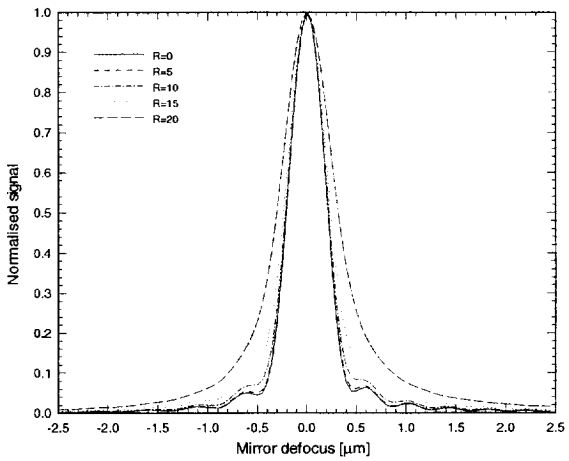

Fig. 4. Axial scans of the detected signal for a coherent detector. The radius of the detector is given in μm.

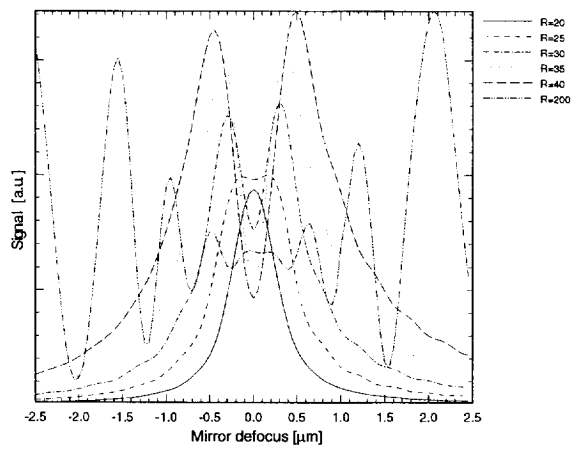

Fig. 6. Axial scans corresponding to a coherent detector. Note that individual curves are not normalised. The detector radius is given in μm.

an essentially similar behaviour than Fig. 3(b) but for the coherent case the curve widths being slightly wider. Indeed, direct comparison (Fig. 5) of curves corresponding to a coherent point detector (dashed line) and an incoherent $d = 5$ μm detector (continuous line) shows that there are no detectable differences between these two cases. The two axial responses in this figure have been plotted in such a way that a vertical offset was added to the incoherent distribution in order to be able to show both of the curves which, otherwise, would have perfectly overlapped.

The effect of increasing the detector size on the detected coherent signal is shown in Fig. 6. The individual curves were *not* normalised for this case. The distribution corresponding to a detector radius of $R = 20$ μm exhibits the usual distribution, but for $R = 25$ μm detector radius we find a developing 'negative' peak in the focal plane. This peak is more pronounced for detector radii larger than 25 μm. When the detector radius reaches the 200 μm value the distribution becomes radically different from that observed for an incoherent detector (distribution is not shown). It is worth pointing out that the absolute signal strength does not increase with increasing detector radius and this eventually leads to a completely vanishing signal when $R \to \infty$.

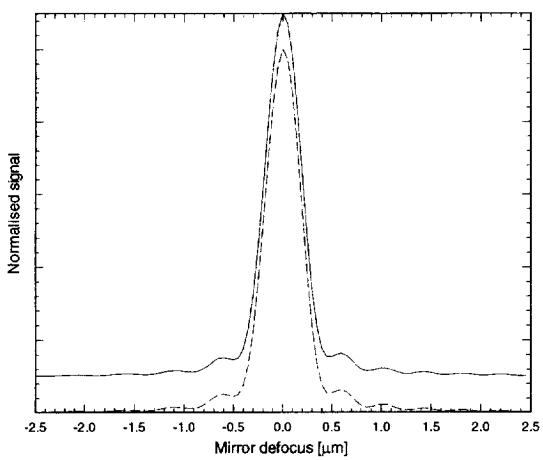

Fig. 5. Comparison of axial scans corresponding to a point-like coherent (dashed line) and a small incoherent detector ($R = 5$ μm, continuous line). Note that an offset was added to the incoherent response for a better comparison.

5. Conclusions

In this paper we have presented, for the first time, a rigorous theory of a scanning optical microscope imaging a plane reflector. We have calculated axial responses with both coherent and incoherent detectors are employed. Our results show that whilst the intensity signal of an incoherent detector is independent of the incident polarisation angle, that of a coherent detector varies with this angle; exhibiting twice as high signal for a 45° incident polarisation than for either 0 or 90° polarisation angle. It is also found that the axial distributions, for both the coherent and incoherent cases, exhibit asymmetric behaviour that confirms previous experimental observations. An analysis of several cases for the asymmetry has been presented. We examined, via numerical examples, how the intensity response of such a microscope varies with increasing detector radius. It has been shown that for small incoherent and point sized coherent detectors the axial responses result in the same distribution. We have also found that when a finite sized coherent detector employed in this system the axial distributions become irregular exhibiting a 'negative' peak for the vicinity of the in-focus position. We have shown that an infinitely large coherent detector would yield a zero signal.

Acknowledgements

The authors would like to thank Professor Colin Sheppard of the University of Sydney, Australia for discussions and for his helpful suggestions. P. Török acknowledges the support from the Wellcome Trust, UK. P. Török is on leave from the Central Research Institute for Physics of the Hungarian Academy of Sciences (Budapest).

References

[1] T. Wilson, ed., Confocal microscopy, 1st Ed. (Academic Press, London, 1990).
[2] T. Dabbs and M. Glass, Appl. Optics 31 (1992) 705.
[3] T. Wilson and A.R. Carlini, Optics Lett. 12 (1987) 227.
[4] T. Wilson and A.R. Carlini, J. Microscopy 149 (1988) 51.
[5] T. Wilson and J.B. Tan, J. Microscopy 182 (1996) 61.
[6] P. Török, P. Varga, Z. Laczik and G.R. Booker, J. Opt. Soc. Am. A 12 (1995) 325.
[7] M. Born and E. Wolf, Principles of Optics, 4th Ed. (Pergamon Press, Oxford, 1970).
[8] E. Wolf, Proc. Roy. Soc. A 253 (1959) 349.
[9] R.K. Luneburg, Mathematical Theory of Optics, 2nd Ed. (Univ. California Press, Berkeley, CA, 1966).
[10] G.N. Watson, A Treatise on the Theory of Bessel Functions, 2nd Ed. (Cambridge University Press, Cambridge, 1952).
[11] A. Walther, The ray and wave theory of lenses, 1st Ed. Cambridge University Press, Cambridge, 1995).
[12] C.J.R. Sheppard and M. Gu, J. Mod. Optics 40 (1993) 1631.
[13] B. Richards and E. Wolf, Proc. Roy. Soc. A 253 (1959) 358.